frontiers | Frontiers in Energy Research

TYPE Original Research
PUBLISHED 02 February 2026
DOI 10.3389/fenrg.2025.1744980

Research on analysis methods for overlapping interference of gas spectral lines in laser photoacoustic spectroscopy

Shi Guang[1], Xie Tao[1], Li Mengqi[1,2], Wang Jie[3], Zhou Zhenqin[1] and Wang Qiaohua[4]*

[1]State Grid Electric Power Research Institute Wuhan Nari Co., Ltd, Wuhan, China, [2]School of Electrical and Electronic Engineering, Huazhong University of Science and Technology, Wuhan, China, [3]Electric Power Science Research Institute State Grid Sichuan Electric Power Company, Chengdu, China, [4]Department of Electrical Engineering, Shanghai Jiao Tong University, Shanghai, China

Check for updates

OPEN ACCESS

EDITED BY
Yani Wang,
Shanghai University of Electric Power, China

REVIEWED BY
Dongxin He,
Shandong University, China
Xi Zhu,
Nanjing Tech University, China

*CORRESPONDENCE
Wang Qiaohua,
qhwang@sjtu.edu.cn

RECEIVED 12 November 2025
REVISED 10 December 2025
ACCEPTED 16 December 2025
PUBLISHED 02 February 2026

CITATION
Guang S, Tao X, Mengqi L, Jie W, Zhenqin Z and Qiaohua W (2026) Research on analysis methods for overlapping interference of gas spectral lines in laser photoacoustic spectroscopy.
Front. Energy Res. 13:1744980.
doi: 10.3389/fenrg.2025.1744980

Laser photoacoustic spectroscopy is employed to measure dissolved gases in transformer oil, which include C_2H_2, C_2H_4, C_2H_6, CH_4, CO_2 and CO. The wavelength of 1532.83 nm was selected as the absorption line for C_2H_2. However, near this wavelength, the absorption line of CO_2 also appears, causing a spectral overlap phenomenon with C_2H_2. An experimental photoacoustic spectroscopy measurement system was established using lasers operating at 1532.83 nm and 1579.6 nm. Driven by a sinusoidal signal, the laser scanned the rising and falling sections of the C_2H_2 Voigt extended line profile at 1532.83 nm. The area under the waveform of the generated photoacoustic signal was calculated via integration. It was found that the influence of CO_2 on the measured C_2H_2 concentration exhibited a specific discrepancy, which was consistent with the ratio of the line profile areas corresponding to the rising and falling sections of the C_2H_2 Voigt profile near 1532.83 nm where CO_2 absorbs. By using the 1579.6 nm laser to measure the CO_2 concentration independently, the portion of the photoacoustic signal area at 1532.83 nm attributable to CO_2—calculated based on the Voigt profile—could be subtracted. This method effectively compensates for the interference in determining the C_2H_2 concentration. Experimental results demonstrate that for various concentration ratios of CO_2 and C_2H_2, the calculated concentrations of both gases after applying this area subtraction method are in good agreement with the expected results. This approach provides a viable solution for addressing interference issues in subsequent multi-gas measurement processes.

KEYWORDS

acetylene, dissolved gas analysis, interference, photoacoustic, tunable laser

1 Introduction

Laser photoacoustic spectroscopy is a mature technology that has been widely applied in various fields, including the analysis of dissolved gases in transformer oil, environmental monitoring, and industrial process gas measurement (Ma et al., 2024; Kireev et al., 2018; Liu et al., 2018). Due to its high sensitivity, high resolution, tunability, and rapid response, this technology has seen rapid development and adoption for detecting dissolved gases in transformer oil (Ma et al., 2025; Huang, 2023).

Tunable Diode Laser Photoacoustic Spectroscopy (TDL-PAS) utilizes the unique "fingerprint" absorption lines of gases at specific wavelengths to perform qualitative and quantitative analysis of their concentrations, with the wavelength scanning method being a commonly used technique. However, during measurement, if multiple strong absorption lines exist at the selected wavelength, the resulting photoacoustic signal can exhibit overlapping peaks, necessitating spectral line separation.

Currently, research on spectral line separation within photoacoustic spectroscopy remains relatively limited. The conventional solution involves seeking an alternative, independent absorption line that is free from interference from other gases, rather than using the line at the overlapping wavelength (Dong et al., 2024). While selecting an absorption line unaffected by interference from the target gas itself is relatively straightforward, finding one free from interference from other gases is considerably more challenging. Therefore, investigating analytical methods to address spectral overlap interference is highly necessary.

In recent years, researchers worldwide have extensively studied the spectral line characteristics of laser absorption spectroscopy. Meng et al. (2015) proposed a software lock-in demodulation technique (SLIDT) to address the spectral overlap of CO and CO_2 near 1581.95 nm. Dong et al. (2024) applied the 2f-SLSM method in TDLAS to separate overlapping spectral lines, effectively improving measurement accuracy when using an interband cascade laser (ICL) to measure CO_2. Yang et al. (2017) investigated a method based on the Partial Least Squares (PLS) algorithm using differential and direct measurement spectra (DS-DMS) to achieve spectral overlap separation, applying it to H_2S gas concentration measurement with a maximum relative error of 2%. Yu et al. (2016) introduced a direct absorption spectral line separation method (DA-SLSM) based on Continuous Wavelet Transform (CWT), linear regression analysis, and Chaotic Particle Swarm Optimization (CPSO), applying it to fiber laser absorption spectroscopy for mixed gases. They achieved high linear correlation coefficients of 0.9996 and 0.9997, with concentration measurement errors for high concentrations of CO and CO_2 not exceeding 0.93% and 1.13%, respectively. Ji et al. (2021), using the H_2O molecule from the HITRAN database as an example, theoretically calculated and simulated absorption spectra under Lorentz, Gauss, and Voigt line profiles using MATHLAB software, analyzing the effects of pressure on H_2O spectral linewidth and peak intensity, as well as the effect of temperature on H_2O absorption. Ma et al. (2004) theoretically analyzed the gas absorption coefficient and provided a general method for its calculation. Ban et al. (2024) investigated measurements of CO_2 in different high-concentration mixtures. On one hand, the absorption linewidth is affected by pressure; reducing pressure can effectively eliminate absorption interference from adjacent lines, presenting a feasible solution for resolving overlapping spectral peaks. On the other hand, the minimum tuning step of a TDLAS system is constrained by its wavelength tuning mechanism, and excessively low pressure can lead to sparse data points in the measured spectrum, thereby affecting the system's detection limit.

This study employs laser photoacoustic spectroscopy, taking the absorption line of C_2H_2 gas at 1532.83 nm as an example, to explore methods for separating the overlapping signals caused by the nearby CO_2 absorption line. First, the parameters of the C_2H_2 and CO_2 absorption lines near 1532.83 nm from the HITRAN 2012 database are discussed. Secondly, a Voigt line profile mathematical model, specifically for the CO_2 Voigt profile, is constructed using LabVIEW programming to calculate the integrated line area contributions of CO_2 within the rising segment and the falling segment of the C_2H_2 line profile at 1532.83 nm. Finally, experiments measuring the concentrations of C_2H_2, CO_2, and their mixture are conducted to validate the feasibility of the aforementioned theoretical analysis, aiming to achieve accurate measurement of C_2H_2 in mixed gas environments.

2 Principle and methods

The photoacoustic effect, the fundamental principle behind Photoacoustic Spectroscopy (PAS), refers to the generation of sound waves resulting from the absorption of modulated or pulsed light by a medium. The underlying physical process can be described as follows. When a gas sample is irradiated by a tunable laser beam whose wavelength coincides with a specific absorption line of the target molecule, the molecules undergo electronic, vibrational, or rotational transitions, absorbing the optical energy and becoming excited (Sigrist, 2003).

Subsequently, these excited molecules return to their ground state primarily through non-radiative relaxation processes, such as collisional de-excitation with other molecules (e.g., N_2, O_2) in the sample. This energy transfer converts the absorbed optical energy into localized translational kinetic energy, effectively generating a transient and periodic temperature increase within the gas. According to the ideal gas law, this temperature rise induces a corresponding periodic pressure change, essentially a localized thermal expansion. Since the incident laser is modulated (e.g., amplitude-modulated), this process repeats periodically, creating a propagating pressure wave—an acoustic wave—at the modulation frequency.

In a typical gas photoacoustic spectrometer, this acoustic wave is detected by a highly sensitive microphone. The electrical signal generated by the microphone is directly proportional to the amplitude of the sound pressure, which in turn is proportional to the number of excited molecules and the incident laser power. Therefore, by measuring the amplitude of this photoacoustic signal while scanning the laser wavelength, one obtains an absorption spectrum. This technique, known as Photoacoustic Spectroscopy, provides a highly sensitive means of performing quantitative and qualitative analysis of trace gases, as the signal strength is directly related to the concentration of the absorbing species (Mandelis and Hess, 2017).

2.1 The calculation method for gas concentration

The Beer-Lambert Law describes the relationship between the concentration of an absorbing species and the attenuation of light through a transparent medium. Its mathematical expression is shown in Equation 1:

$$I/I_0 = exp(-\alpha(\lambda)LC) \tag{1}$$

Where: I is the intensity of the light passing through the sample cell, I_0 is the initial intensity of the light, α the absorptivity or formerly called the extinction coefficient, L is the length of light path, C is the gas concentration in the sample cell.

Tunable Diode Laser Photoacoustic Spectroscopy (TDL-PAS) employs the "Wavelength Scanning Method" for implementation. Leveraging the narrow linewidth (typically less than 10 MHz) and high stability of a Distributed Feedback (DFB) laser, the output wavelength of the tunable semiconductor laser is altered by modifying its operating current and temperature.

Since temperature tuning is relatively slow, TDL-PAS primarily utilizes current modulation to achieve rapid changes in the output wavelength. As the output laser wavelength scans across a gas absorption line, a photoacoustic signal is generated, the profile of which mirrors the shape of the gas absorption line. By periodically modulating the operating current, a periodic photoacoustic signal is produced.

Based on different spectral line broadening mechanisms, the line profile can be categorized into three types. Under high-pressure conditions, where collisional broadening is dominant, the Lorentzian profile is used. In low-pressure environments, where Doppler broadening (and natural broadening) becomes significant, the line shape is primarily described by the Gaussian profile. Typically, since both broadening mechanisms coexist, neither the Gaussian nor the Lorentzian profile alone can adequately describe the absorption line. Therefore, a third line profile, known as the Voigt profile, is employed. The Voigt profile provides a more accurate description, as it is formulated as the convolution of the Lorentzian and Gaussian profiles (Yin et al., 2013).

In this study, by periodically scanning the absorption minimum and maximum, a periodic photoacoustic signal S is generated. The microphone detects the changes in the photoacoustic signal (Zhang et al., 2018). This process can be expressed mathematically as follows:

$$S = (S_m C_{cell} P_\lambda \alpha) \cdot C \tag{2}$$

Where: S_m is the sensitivity of the microphone, C_{cell} is the photoacoustic cell constant, which is determined by the cell's geometry and material properties, P_λ denotes the incident optical power, α is the absorption coefficient of the gas molecules at the incident light wavelength, C the concentration of the target gas.

In the implementation of photoacoustic spectroscopy based on the wavelength scanning method of a tunable laser, when S_m and C_{cell} are held constant, the amplitude of the photoacoustic signal is determined by P_λ, α and C. Here P_λ is related to the laser drive current and exhibits a linear relationship with it. The absorption coefficient α_λ is governed by the gas molecular absorption line shape, which is typically represented by the Voigt profile. By modulating the optical power P_λ (e.g., via the laser current) and scanning the wavelength across the gas absorption line shape α_λ, a distinct photoacoustic signal waveform is generated (Wang et al., 2025).

Based on the Voigt profile of C_2H_2 at 1532.83 nm retrieved from the HITRAN database, as shown in Figure 1, the photoacoustic signal generated by the wavelength scanning method is linearly proportional to the product of the laser output power and the absorption line intensity at the corresponding wavelength, according to Equation 2.

The integrated area under the scanned waveform, which constitutes the area of the output signal, is given by:

$$\boldsymbol{\varphi}_\Delta = \int_{\lambda_{ss}}^{\lambda_{se}} \boldsymbol{S d\lambda} = \boldsymbol{S_m C_{cell} \cdot C} \int_{\lambda_{ss}}^{\lambda_{se}} \boldsymbol{P_\lambda(i)} \mathrm{V}(\lambda, \lambda_0) \boldsymbol{d\lambda} \tag{3}$$

where: λ_{ss} and λ_{se} represent the starting and ending wavelengths generated by the laser scanning current, respectively.

As indicated in Equation 3, the Voigt line profile remains essentially constant under standard temperature and pressure but lacks a simple analytical form (Zhang et al., 2018). Since the photoacoustic signal at each point is linearly proportional to the product of the laser output power and the absorption line intensity at that specific wavelength, the integrated area under the photoacoustic signal waveform is consequently proportional to the integral of the product of the laser power curve and the gas absorption line profile over the scanned wavelength interval.

From Equation 3, it can be concluded that for a fixed wavelength scanning interval, the Voigt line profile of the gas is constant, and the laser output power curve is maintained, $\boldsymbol{K(\lambda)} = \int_{\lambda_{ss}}^{\lambda_{se}} \boldsymbol{P_\lambda(i)} \mathrm{V}(\lambda, \lambda_0) \boldsymbol{d\lambda}$, S_m and C_{cell} are constant. Therefore, the integrated signal area for a specific gas under these stable conditions is linear to the gas concentration. Due to variations in laser output power, the waveform of the gas photoacoustic signal does not perfectly match the Voigt line profile.

2.2 LabVIEW simulation of a voigt profile mathematical model

The line shape function V(λ) of an absorption spectral line represents the variation of the absorption rate of the spectral line with optical frequency. This paper discusses the absorption spectral lines of C_2H_2 and CO_2 under constant temperature and pressure, both of which conform to the Voigt line shape model (Tian et al., 2023).

The Voigt line shape function is expressed in an integral form and lacks an easily computable analytical expression. Its integral form is related to the half-widths of the Lorentzian and Doppler line shapes.

$$\begin{aligned} \boldsymbol{g_z(\lambda, \lambda_0)} = \boldsymbol{V(\lambda, \lambda_0)} &= \int_{-\infty}^{+\infty} \boldsymbol{g_L(\lambda_1, \lambda_0) . g_D(\lambda, \lambda_1) d\lambda_1} \\ &= \sqrt{\frac{\boldsymbol{ln\,2}}{\boldsymbol{\pi}}} \frac{\boldsymbol{1}}{\boldsymbol{\alpha_D}} \left(\frac{\boldsymbol{\mu}}{\boldsymbol{\pi}} \int_{-\infty}^{+\infty} \frac{\boldsymbol{1}}{\boldsymbol{(\xi + t)^2 + \mu^2}} \boldsymbol{e^{-t^2} dt} \right) \end{aligned} \tag{4}$$

Where: α_D is the half-width of Doppler profile, α_L the half-width of the Lorentzian profiles, $\xi = \sqrt{ln\,2}\frac{\lambda\text{-}\lambda_0}{\alpha_D}$, $\mu = \sqrt{ln\,2}\frac{\alpha_L}{\alpha_D}$, $t = \frac{\sqrt{ln\,2}}{\alpha_D}(\lambda_1 - \lambda)$, λ_1 is the central wavelength, λ_0 is the central wavelength of the profile.

Equation 4, when corrected to the second-order approximation, becomes:

$$\begin{aligned} \mathrm{g_z}(\lambda, \lambda_0) = 0.0016\left(1 - \frac{\alpha_L}{\alpha_V}\right)\frac{\alpha_L}{\alpha_V} \cdot \left[e^{-0.4\left(\frac{\lambda\text{-}\lambda_0}{2\alpha_V}\right)^{2.25}} - \frac{10}{10 + \left(\frac{\lambda\text{-}\lambda_0}{2\alpha_V}\right)^{2.25}} \right] \\ + \left(1 - \frac{\alpha_L}{\alpha_V}\right) e^{-2.772\left(\frac{\lambda\text{-}\lambda_0}{2\alpha_V}\right)^2} + \frac{\alpha_L}{\alpha_V} \frac{1}{1 + 4\left(\frac{\lambda\text{-}\lambda_0}{2\alpha_V}\right)^2} \end{aligned} \tag{5}$$

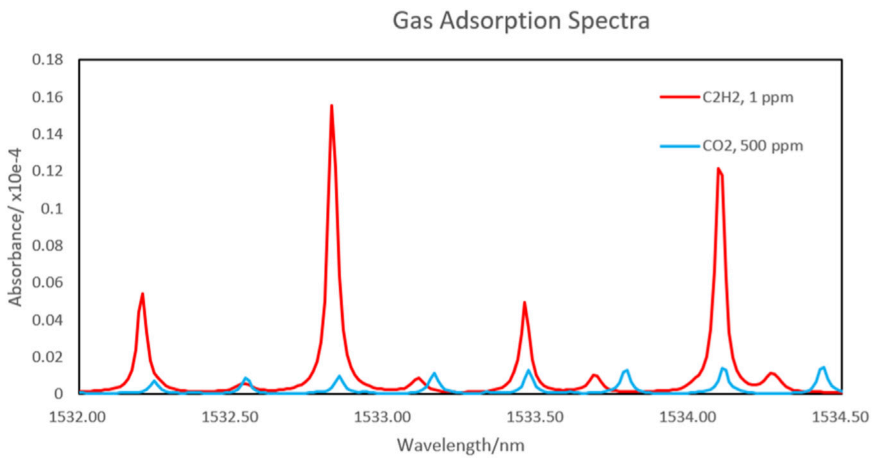

FIGURE 1
Voigt profile of C_2H_2 and CO_2.

Where: α_V is the half-width of the Voigt profiles, and can be expressed as:

$$\alpha_V = 0.5\left(1.0692\alpha_L + \sqrt{0.86639\alpha_L{}^2 + 4\alpha_D{}^2}\right) \tag{6}$$

The normalized Voigt line shape has an area of 1, and the product of the absorption peak height and the normalized Voigt line shape area corresponds to the integrated area under the Voigt line shape for each gas at a specific wavelength. Under isolated absorption lines, the peak height is proportional to the gas concentration; however, in the presence of overlapping gas spectral lines, the peak height alone cannot be directly correlated with gas concentration.

The Voigt line profile is simulated using Equation 5 and Equation 6, and the area under the Voigt profile is obtained by computing over different wavelength ranges. The area under the Voigt profile can be calculated using numerical integration methods. By discretizing the Voigt function into grid points, the area is evaluated via numerical integration techniques, such as Simpson's rule or the trapezoidal rule as shown in Equation 7.

$$Area = \sum_{i=0}^{n} \frac{g_z(\lambda_{i-1}, \lambda_0) + g_z(\lambda_i, \lambda_0)}{2} \cdot \Delta\lambda \tag{7}$$

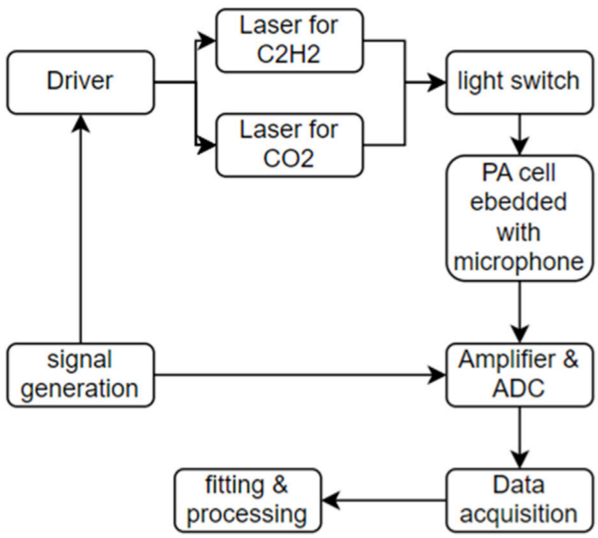

FIGURE 2
Schematic diagram of laser photoacoustic spectroscopy.

2.3 Analysis method for overlapping spectral lines

According to Equation 3, the laser is driven by Pλ(i) in a sinusoidal manner. When the sinusoidal wave modulates the laser wavelength over the range of 1532.68 nm–1532.83 nm, it captures the rising edge of the C_2H_2 Voigt line shape. This modulation method is illustrated in Figure 1. This specific wavelength range also encompasses a portion of the broadened Voigt line profile of CO_2 (Wang et al., 2025). Conversely, when the modulation range is 1532.83 nm–1532.98 nm, the falling edge of the C_2H_2 Voigt line shape is captured, as shown in Figure 2, and this range similarly covers another part of the extended CO_2 Voigt line profile.

This approach enables the complete calculation of the integrated area under the C_2H_2 Voigt profile, as well as the partial areas under the CO_2 Voigt profile. The analysis of these overlapping peaks can be essentially treated as the superposition of the Voigt profile areas from both C_2H_2 and CO_2 gases.

Quantitative analysis via LabVIEW indicates that the CO_2 Voigt profile area within the 1532.68 nm–1532.83 nm range constitutes 39% of the total area of the extended CO_2 absorption line profile centered at 1532.85 nm. The area in the 1532.83 nm–1532.98 nm range constitutes the remaining 61%.

Employing peak height as a substitute for integrated area in the analysis of overlapping spectral lines can lead to significant computational errors (Meng et al., 2015; Rieker et al., 2009). As shown in Figure 3, the absorption line shapes of C_2H_2 and CO_2

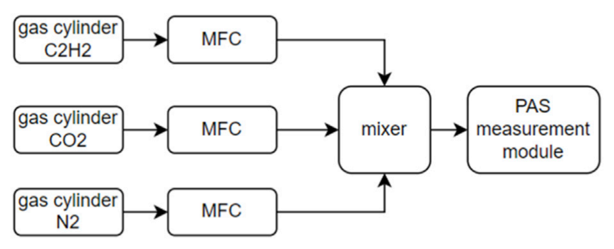

FIGURE 3
The experimental setup.

do not completely overlap in the 1532.68 nm–1532.98 nm region, resulting in partially overlapping photoacoustic signals. When the C_2H_2 signal is dominant, its peak height is located at 1532.83 nm. When the CO_2 signal is dominant, its peak appears at 1532.85 nm. Furthermore, the broadened line shape of CO_2 influences the peak height at 1532.83 nm. Consequently, relying solely on peak height to resolve these overlapping peaks yields unsatisfactory results.

3 Experimental results and discussion

3.1 Instrument

The schematic diagram of the experimental principle and the setup for laser photoacoustic spectroscopy is shown in Figure 2. The measurement employs the photoacoustic signal method, which requires the laser output frequency to be scanned over a specific range. The experimental procedure is as follows: first, a sinusoidal sweep signal generated by a signal generator is used to drive the DFB laser via a laser driver module. The laser output is then directly coupled into the photoacoustic cell using an optical fiber coupler.

To accommodate the limited gas sample volume typically available in field installations of transformer DGA (Dissolved Gas Analysis) monitoring, a non-resonant photoacoustic cell design is adopted. Within the cylindrical cavity of the cell, the laser beam undergoes multiple reflections between two mirrors, allowing the gas sufficient interaction with the emitted light.

When the laser wavelength matches the specific absorption wavelength of acetylene (C_2H_2), the gas molecules absorb photons and undergo transitions to higher energy levels. As the laser scans away from this wavelength, the excited molecules return to their ground state or lower energy levels, releasing the previously absorbed energy, typically in the form of heat. This energy release causes a localized temperature increase in the gas, leading to thermal expansion. Consequently, the pressure within the photoacoustic cell fluctuates, and these changes are detected as photoacoustic signals by a microphone.

The experimental system employs two tunable DFB lasers, OC45310SMF for C_2H_2 and OC45850SMF for CO_2 (Qianlian Technology, China). By tuning the temperature and current parameters, the lasers output central wavelength of 1532.83 and 1579.6 nm respectively. The 1579.6 nm wavelength was selected for CO_2 measurement as it corresponds to a strong, isolated absorption line that is free from spectral interference by C_2H_2 and other dissolved gases of interest (C_2H_4, C_2H_6, CH_4, CO), ensuring an independent and accurate reference measurement. To accommodate the small gas sample volumes typical in transformer DGA applications, the photoacoustic cell is designed as a non-resonant cavity made of brass. The internal shape of the cavity is cylindrical, with a volume of 5 mL, and the inner walls are polished and gold-plated to minimize adsorption and maximize reflection (Sur et al., 2016). A microphone is equipped within the photoacoustic cavity, model GRAS 40AD-FV1/2' (GRAS Sound and Vibration A/S, Denmark), with a response frequency range of 3.15 Hz–10 kHz. The data acquisition device is an NI9181 (National Instruments, United States). The laser driver, signal generator, lock-in amplifier, and control software are all custom-developed programs.

3.2 Experiment on C_2H_2 PA signal

To generate the different concentrations of C_2H_2, CO_2 and the mixture of these two gases, a dilution system is setup, as Figure 3 demonstrated, to dilute cylinder gas of C_2H_2 and CO_2 with pure N_2 to the desired concentrations.

Varying concentrations of acetylene (C_2H_2) — specifically 1, 5, 10, 20, 50, 100, 200, and 500 ppm—were prepared. Different photoacoustic signal amplitudes were obtained through experimental measurements using the apparatus.

The current driving the C_2H_2 laser was adjusted to generate infrared output spanning from 1532.68 nm to 1532.83 nm, a wavelength range that covers the rising edge of the C_2H_2 Voigt line shape. Similarly, the drive current was modified to produce output from 1532.83 nm to 1532.98 nm, corresponding to the falling edge of the C_2H_2 Voigt line shape. The photoacoustic signal was quantified using both the peak height and the integrated profile area methods. The corresponding numerical values are summarized in Table 1, and the resulting calibration curves are presented in Figure 4.

The coefficient of determination (R^2) was calculated for each method. The R^2 value for the peak height method was found to be lower than that for the profile area method, indicating that the profile area exhibits superior linearity compared to the peak height. In the current setup utilizing a non-resonant photoacoustic cell, the detection limit for C_2H_2 at the ppm level is primarily constrained by the intrinsic acoustic and vibration noise floor of the cell. While resonant cell or quartz tuning fork (QTF) based designs offer paths to significantly lower detection limits, the present non-resonant design prioritizes robustness, compactness, and compatibility with the small gas sample volumes typical in field-deployed transformer DGA monitors.

As shown in Table 1, the photoacoustic signal values corresponding to the falling edge section are larger. This is primarily attributed to the higher drive current required for the 1532.83 nm–1532.98 nm range compared to the 1532.68 nm–1532.83 nm range, which is consistent with the photoacoustic signal calculation principle described by Equation 3.

PA signal1 represents the PA signal obtained by scanning the laser wavelength over the rising edge of the C_2H_2 Voigt line shape and calculating the integrated profile area.

TABLE 1 PA signals at different C_2H_2 concentrations.

Gas concentration/ppm	PA signal1/μV	PA signal2/μV	PA signal3/μV	PA signal4/μV
1	5.37	7.06	3.46	4.56
5	22.89	29.37	14.32	18.11
10	48.58	62.83	36.95	48.54
20	85.32	115.57	57.01	74.99
50	233.00	317.00	148.17	189.88
100	460.68	595.65	361.60	462.18
200	833.16	1202.19	660.25	848.60
500	2377.84	3443.11	1456.91	1879.13

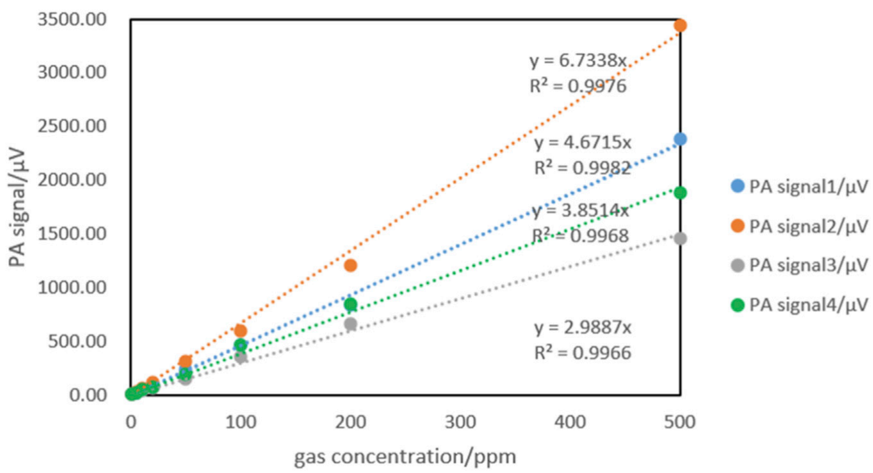

FIGURE 4
Relationship between the gas concentration and PA signal.

PA signal2 represents the PA signal obtained by scanning the laser wavelength over the falling edge of the C_2H_2 Voigt line shape and calculating the integrated profile area.

PA signal3 represents the PA signal obtained by scanning the laser wavelength over the rising edge of the C_2H_2 Voigt line shape and calculating the peak height.

PA signal4 represents the PA signal obtained by scanning the laser wavelength over the falling edge of the C_2H_2 Voigt line shape and calculating the peak height.

3.3 Experiment on CO_2 PA signal

Varying concentrations of CO_2—respectively 100, 200, 500, 1000, 5000, 10,000, and 50,000 ppm—were prepared. PA signals were measured by driving two lasers respectively.

The current of the C_2H_2 laser was adjusted to generate infrared output in the range of 1532.68 nm–1532.83 nm, which scans the rising edge of the C_2H_2 Voigt line shape. Similarly, the current was modified to produce output from 1532.83 nm to 1532.98 nm, scanning the falling edge of the C_2H_2 Voigt line shape. The integrated profile area method was employed to calculate the respective PA signal values, and the results are summarized in Table 2. The corresponding calibration curves are shown in Figure 5. The peak height method was employed to calculate the respective PA signal values, and the results are summarized in Table 3. The corresponding calibration curves are shown in Figure 6.

In the data presented in Table 2, the photoacoustic signal from the CO_2 absorption peak at 1532.85 nm was weak at lower concentrations and thus not distinct. However, when the concentration exceeded 5,000 ppm, the photoacoustic signal exhibited a regular periodic pattern. A comparison of the signals obtained under the 1532.83 nm–1532.98 nm drive and the 1532.68 nm–1532.83 nm drive revealed that the CO_2 signal in the 1532.83 nm–1532.98 nm range was significantly stronger. Experimental results indicated that the photoacoustic signal in this range accounted for approximately 64% of the total relevant signal. This observed dominance is consistent with

TABLE 2 PA signals at different CO_2 concentrations calculated the integrated profile area.

Gas concentration/ppm	PA signal5/μV	PA signal6/μV	PA signal7/μV	PA signal8/μV
100	8.5	0.12	8.37	0.12
200	11.9	0.02	11.96	−0.02
500	34.3	0.16	30.17	0.06
1000	86.21	0.28	87.1	0.03
5000	552.34	0.69	598.7	2.15
10,000	1011.92	2.5	1080.68	6.69
50,000	4896.93	14.27	5001.07	41.75

TABLE 3 PA signals at different CO_2 concentrations calculated the peak height.

Gas concentration/ppm	PA signal9/μV	PA signal10/μV	PA signal11/μV	PA signal12/μV
100	6.82	0.11	6.1	0.03
200	10.81	0.25	7.74	−0.22
500	36.44	−0.17	34.49	0.26
1000	75.29	0.01	72.52	0.44
5000	427.31	0.82	419.19	3.25
10,000	910.87	2.07	879.96	6.95
50,000	3831.54	11.96	3837.53	34.37

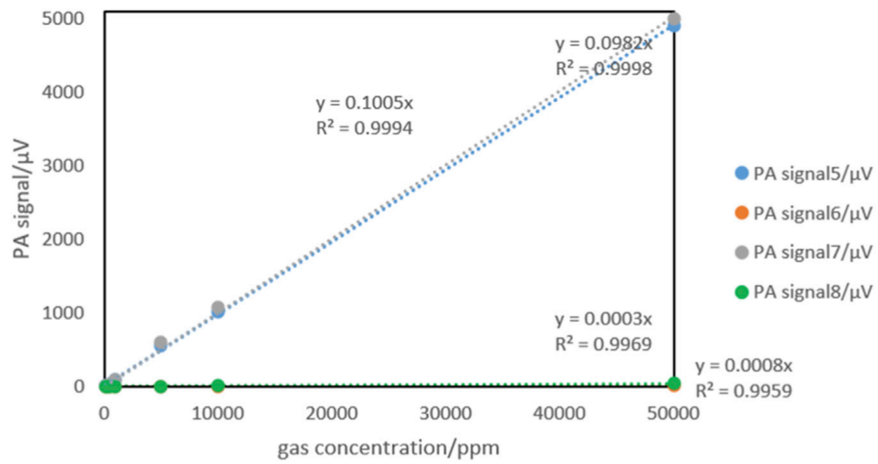

FIGURE 5
Relationship between the gas concentration and PA signal.

the higher laser output power in the 1532.83 nm–1532.98 nm range and aligns substantially with the area calculation results obtained from LabVIEW simulations.

PA signal5 represents the PA signal obtained by scanning the CO_2 laser wavelength over the rising edge of the C_2H_2 Voigt line shape and calculating the integrated profile area.

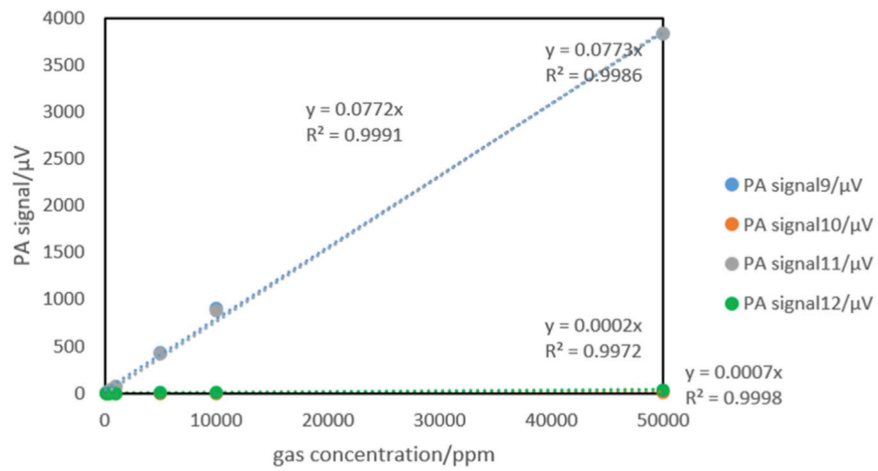

FIGURE 6
Relationship between the gas concentration and PA signal.

PA signal6 represents the PA signal obtained by scanning the C_2H_2 laser wavelength over the rising edge of the C_2H_2 Voigt line shape and calculating the integrated profile area.

PA signal7 represents the PA signal obtained by scanning the CO_2 laser wavelength over the falling edge of the C_2H_2 Voigt line shape and calculating the integrated profile area.

PA signal8 represents the PA signal obtained by scanning the C_2H_2 laser wavelength over the falling edge of the C_2H_2 Voigt line shape and calculating the integrated profile area.

PA signal9 represents the PA signal obtained by scanning the CO_2 laser wavelength over the rising edge of the C_2H_2 Voigt line shape and calculating the peak height.

PA signal10 represents the PA signal obtained by scanning the C_2H_2 laser wavelength over the rising edge of the C_2H_2 Voigt line shape and calculating the peak height.

PA signal11 represents the PA signal obtained by scanning the CO_2 laser wavelength over the falling edge of the C_2H_2 Voigt line shape and calculating the peak height.

PA signal12 represents the PA signal obtained by scanning the C_2H_2 laser wavelength over the falling edge of the C_2H_2 Voigt line shape and calculating the peak height.

The signal ratio of CO_2 between the C_2H_2 and CO_2 lasers was calculated by selecting the last three representative sets of data, thereby obtaining the compensation coefficient of CO_2 for C_2H_2. When the PA signal was calculated using the integrated profile area, the compensation coefficient was 0.0031 for the wavelength scan over the rising edge of the C_2H_2 Voigt line shape, and 0.009 for the scan over the falling edge. When the PA signal was calculated using the peak height, the compensation coefficient was 0.0033 for the wavelength scan over the rising edge of the C_2H_2 Voigt line shape, and 0.0092 for the scan over the falling edge. It can be concluded that with either calculating method, the signal ratio of CO_2 between the C_2H_2 and CO_2 is very close, determined by the scan region of laser.

3.4 Experiment on mixture PA signal

Gas mixtures with the following compositions were prepared: 1 ppm C_2H_2 and 100 ppm CO_2, 1 ppm C_2H_2 and 200 ppm CO_2, 1 ppm C_2H_2 and 1,000 ppm CO_2,1 ppm C_2H_2 and 5000 ppm CO_2, 1 ppm C_2H_2 and 10,000 ppm CO_2, and 1 ppm C_2H_2 and 50,000 ppm CO_2. Following the method described in Section 3.2, the photoacoustic signals under the drive of the two lasers were measured. The photoacoustic C_2H_2 signal values are shown in Figure 7. The corresponding numerical data calculated using both the integrated signal area and the peak height methods are summarized in Table 4.

PA signal13 represents the PA signal obtained by scanning the C_2H_2 laser wavelength over the rising edge of the C_2H_2 Voigt line shape and calculating the integrated profile area, shown as Figure 7a.

PA signal14 represents the PA signal obtained by scanning the C_2H_2 laser wavelength over the falling edge of the C_2H_2 Voigt line shape and calculating the integrated profile area, shown as Figure 7b.

PA signal15 represents the PA signal obtained by scanning the C_2H_2 laser wavelength over the rising edge of the C_2H_2 Voigt line shape and calculating the peak height, shown as Figure 7c.

PA signal16 represents the PA signal obtained by scanning the C_2H_2 laser wavelength over the falling edge of the C_2H_2 Voigt line shape and calculating the peak height, shown as Figure 7d.

As shown in Figure 1, the central frequencies of the C_2H_2 and CO_2 spectral lines slightly differ. According to the HITRAN 2012 database, the central frequency of the C_2H_2 line is located at 1532.83 nm, while that of the CO_2 line is at 1532.85 nm.

In the wavelength sweep range of 1532.68 nm–1532.83 nm, both C_2H_2 and CO_2 exhibit similar rising-edge line shapes. When driven by a sinusoidal waveform, the superimposed photoacoustic signals share the same phase direction, resulting in nearly identical peak positions.

In the sweep range of 1532.83 nm–1532.98 nm, when the CO_2 concentration in the mixed gas is below 10,000 ppm, the photoacoustic signal is dominated by C_2H_2, with a superimposed contribution from the broadened CO_2 profile. Nevertheless, the

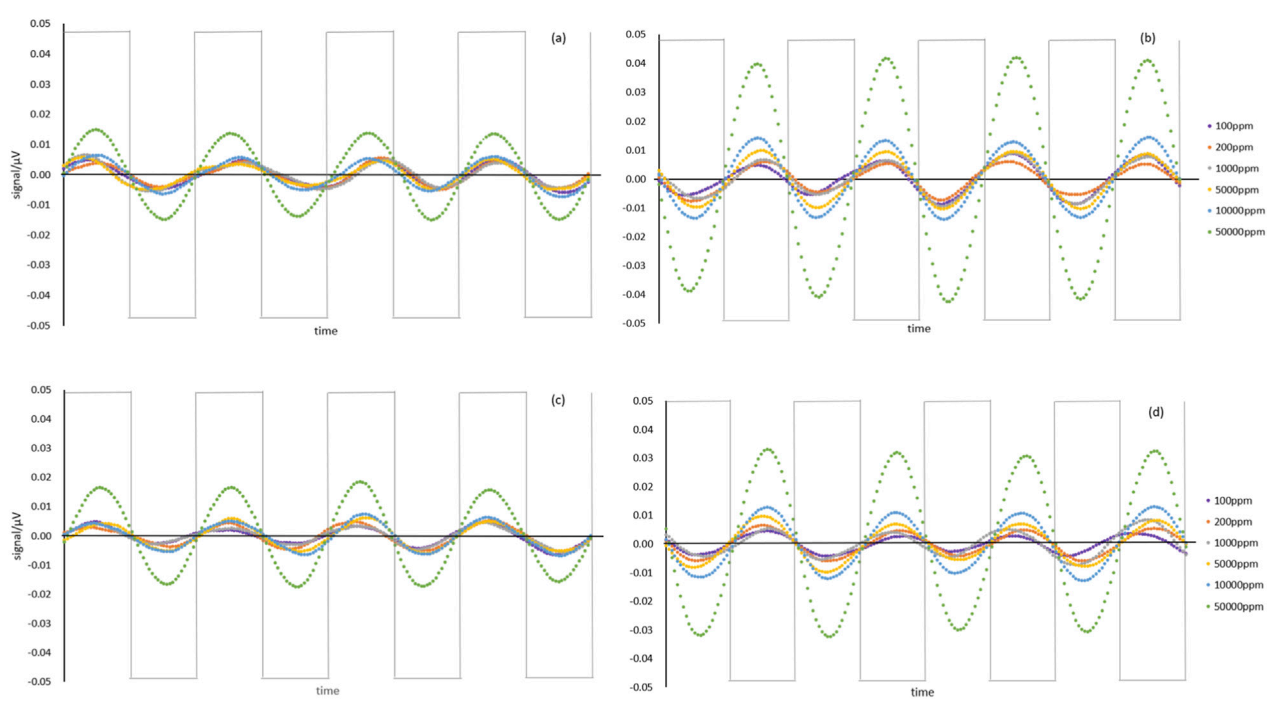

FIGURE 7
C_2H_2 PA signals of different gas mixtures which C_2H_2 1 ppm and CO_2 100/200/1000/5000/10,000/50,000 ppm respectively. **(a)** Integrated profile area calculated from the rising edge of the C_2H_2 Voigt line shape; **(b)** integrated profile area calculated from the falling edge of the C_2H_2 Voigt line shape; **(c)** peak height calculated from the rising edge of the C_2H_2 Voigt line shape; **(d)** peak height calculated from the falling edge of the C_2H_2 Voigt line shape.

TABLE 4 PA signals of C_2H_2 at different mixture concentrations with CO_2 correction off/on.

C_2H_2/CO_2 mixture concentration/ppm	PA signal13/μV		PA signal14/μV		PA signal15/μV		PA signal16/μV	
CO_2 correction	OFF	ON	OFF	ON	OFF	ON	OFF	ON
1/100	4.7	4.67	6.59	6.51	2.72	2.70	3.71	3.65
1/200	4.64	4.60	6.73	6.62	2.97	2.93	3.49	3.42
1/1000	4.78	4.67	6.65	6.38	2.55	2.43	3.87	3.55
1/5000	4.9	4.63	7.68	6.90	2.73	2.48	4.15	3.48
1/10,000	6.31	4.60	12.16	6.77	4.54	3.13	7.96	4.10
1/50,000	8.12	4.98	16.7	6.97	6.23	3.22	11.66	3.56

peak positions remain largely consistent. However, when the CO_2 concentration exceeds 10,000 ppm, the signal becomes dominated by CO_2, with an additional contribution from the broadened C_2H_2 profile. In this case, the peak position differs from the previous scenario, which can be clearly seen in Figure 7d. This variation introduces inaccuracies when using peak height for gas concentration quantification. Directly applying the peak height subtraction method described in Section 3.2 yields results that deviate from those obtained in Section 3.1.

In contrast, when the integrated profile area is used for concentration calculation, the peak position becomes irrelevant. Based on the principle of waveform superposition, the actual C_2H_2 photoacoustic signal profile area can be directly determined by calculating the contribution of CO_2 in Section 3.2 at each concentration. The values obtained using this method are in strong agreement with the C_2H_2 measurement results from Section 3.1.

Gas mixtures with the following compositions were prepared: 10 ppm C_2H_2 and 100 ppm CO_2, 10 ppm C_2H_2 and 200 ppm CO_2, 10 ppm C_2H_2 and 1000 ppm CO_2, 10 ppm C_2H_2 and 5000 ppm CO_2, 10 ppm C_2H_2 and 10,000 ppm CO_2, and 10 ppm C_2H_2 and 50,000 ppm CO_2. The experiments were repeated according to the aforementioned procedure, yielding the results summarized

TABLE 5 PA signals of C_2H_2 at different mixture concentrations with CO_2 correction off/on.

C_2H_2/CO_2 mixture concentration/ppm	PA signal17/μV		PA signal18/μV		PA signal19/μV		PA signal20/μV	
CO_2 correction	OFF	ON	OFF	ON	OFF	ON	OFF	ON
10/100	46.87	46.84	68.11	68.03	30.8	30.78	37.81	37.75
10/200	46.74	46.70	68.18	68.07	31.38	31.36	37.54	37.47
10/1000	47.43	47.16	70.47	69.69	31.87	31.62	39.3	38.58
10/5000	48.62	46.91	74.17	68.78	32.23	31.42	43.52	41.18
10/10,000	49.91	46.77	76.74	67.01	32.85	30.96	46.23	40.67
10/50,000	62.34	47.16	111.81	66.80	40.74	28.10	76.43	38.35

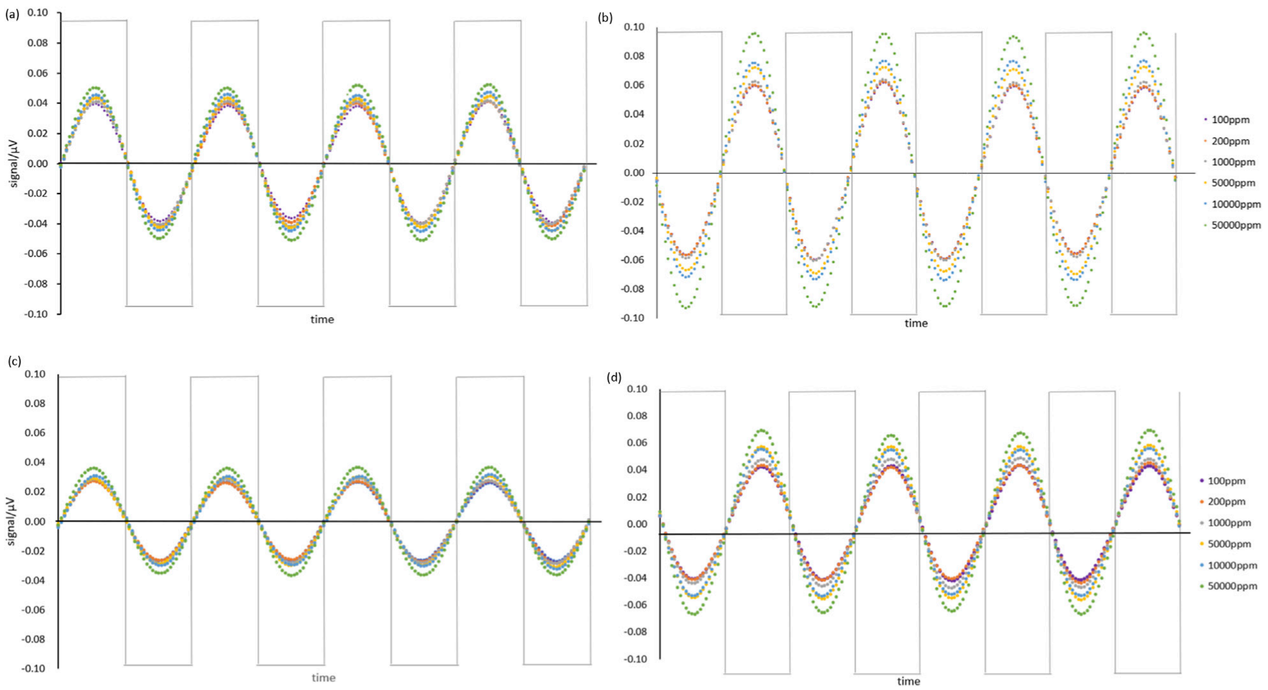

FIGURE 8
C2H2 PA signals of different gas mixtures which C2H2 10 ppm and CO_2 100/200/1000/5000/10,000/50,000 ppm respectively. **(a)** Integrated profile area calculated from the rising edge of the C_2H_2 Voigt line shape; **(b)** integrated profile area calculated from the falling edge of the C_2H_2 Voigt line shape; **(c)** peak height calculated from the rising edge of the C_2H_2 Voigt line shape; **(d)** peak height calculated from the falling edge of the C_2H_2 Voigt line shape.

in Table 5. The corresponding signal curves are shown in Figure 8.

PA signal17 represents the PA signal obtained by scanning the C_2H_2 laser wavelength over the rising edge of the C_2H_2 Voigt line shape and calculating the integrated profile area shown as Figure 8a.

PA signal18 represents the PA signal obtained by scanning the C_2H_2 laser wavelength over the falling edge of the C_2H_2 Voigt line shape and calculating the integrated profile area shown as Figure 8b.

PA signal19 represents the PA signal obtained by scanning the C_2H_2 laser wavelength over the rising edge of the C_2H_2 Voigt line shape and calculating the peak height shown as Figure 8c.

PA signal20 represents the PA signal obtained by scanning the C_2H_2 laser wavelength over the falling edge of the C_2H_2 Voigt line shape and calculating the peak height shown as Figure 8d.

It can be concluded that when the signal of C_2H_2 exceeds 10ppm, it becomes the dominant part of the total signal and the maximum value consistently occurs at the central absorption wavelength of C_2H_2.

The presented area-subtraction method provides a distinct approach compared to other techniques for handling spectral interference. Methods based on computational algorithms, such as Partial Least Squares (PLS), can effectively deconvolve overlapping spectra but require extensive calibration datasets spanning the entire concentration space of all interfering components. Harmonic detection techniques like the second harmonic spectral line separation method (2f-SLSM) are powerful but can be complex to implement and optimize. In contrast, the physical-model-driven method proposed here, based on the direct calculation and subtraction of the interfering Voigt profile area, is conceptually straightforward and requires only a one-time calibration to determine the fixed area ratio coefficients for a known, specific interference pair. This makes it particularly suitable for embedding into dedicated hardware for real-time, continuous monitoring applications where the interfering species are well-defined, as is often the case in transformer gas analysis.

4 Conclusion

This study investigates the overlapping absorption peaks of C_2H_2 and CO_2 near 1532.83 nm. The Voigt profile area was simulated using LabVIEW, and the magnitude of CO_2 interference on the C_2H_2 signal was quantified by analysing the distinct wavelength intervals of 1532.68 nm–1532.83 nm and 1532.83 nm–1532.98 nm. An experimental system was constructed to validate the findings, employing wavelength scans across these intervals. Results demonstrated a discernible difference in the interference effect of CO_2 on the detected C_2H_2 concentration between the two scanning ranges.

Furthermore, the photoacoustic signals from gas mixtures were evaluated using both peak height and integrated profile area methods. In peak height analysis, the differing central frequencies of the overlapping peaks led to shifts in the observed peak positions, making it difficult to reliably resolve the spectral interference. In contrast, the integrated profile area method produced results consistent with the LabVIEW simulations, demonstrating its effectiveness in mitigating measurement errors caused by overlapping gas peaks in photoacoustic spectroscopy. The algorithmic simplicity of calculating and subtracting a fixed fraction of an independently measured interference signal makes this method highly suitable for implementation in embedded systems, enabling automated, real-time correction in field-deployed DGA monitors. Furthermore, the general framework—using an independent laser line for the interfering species and subtracting its calculated contribution based on a pre-characterized spectral profile—constitutes a viable and practical strategy for addressing similar specific spectral overlaps in multi-gas measurement scenarios.

Data availability statement

The raw data supporting the conclusions of this article will be made available by the authors, without undue reservation.

Author contributions

SG: Writing – original draft, Data curation, Methodology. XT: Writing – original draft, Investigation, Methodology. LM: Writing – review and editing, Data curation. WJ: Writing – review and editing, Methodology. ZZ: Investigation, Writing – review and editing. WQ: Supervision, Writing – review and editing.

Funding

The author(s) declared that financial support was received for this work and/or its publication. This study was generously supported by the Science and Technology fund of State Grid Corporation of China, under contract No. 5500-202340529A-3-2-ZN.

Conflict of interest

Authors SG, XT, LM, and ZZ were employed by State Grid Electric Power Research Institute Wuhan NARI Co., Ltd. Author WJ was employed by Electric Power Science Research Institute State Grid Sichuan Electric Power Company.

The remaining author(s) declared that this work was conducted in the absence of any commercial or financial relationships that could be construed as a potential conflict of interest.

The authors declare that this study received funding from State Grid Corporation of China. The funder was not involved in the study design, collection, analysis, interpretation of data, the writing of this article, or the decision to submit it for publication.

Generative AI statement

The author(s) declared that generative AI was not used in the creation of this manuscript.

Any alternative text (alt text) provided alongside figures in this article has been generated by Frontiers with the support of artificial intelligence and reasonable efforts have been made to ensure accuracy, including review by the authors wherever possible. If you identify any issues, please contact us.

Publisher's note

References

Ban, D., Li, N., Zheng, Y., and Xue, C. (2024). CO_2 measurement under different pressure and vibration conditions using tunable diode laser absorption spectroscopy. *Photonics* 11 (2), 146. doi:10.3390/photonics11020146

Dong, W., Chen, C., Li, Z., Wang, Y., Piao, H., and Wang, P. (2024). Improving the accuracy using second harmonic spectral line separation method for mid-infrared CO2 sensing system. *IEEE Trans. Instrum. Meas.* 73, 1–9. doi:10.1109/TIM.2024.3370787

Huang, Z. (2023). The on-line detection technology of dissolved gases in transformer oil based on photoacoustic spectroscopy. *Anal. Instrum.* (5), 1–7. doi:10.3969/j.issn.2095-4956.2023.05.001

Ji, H. Y., Qu, D. S., Hong, Y. J., and Zhu, X. H. (2021). Measurements of H_2O spectroscopic parameters based on the tunable diode laser absorption spectroscopy. *Spectrosc. Spectr. Analysis* (4), 1072–1078. doi:10.3964/j.issn.1000-0593(2021)04-1072-07

Kireev, S. V., Kondrashov, A. A., and Shnyrev, S. L. (2018). Improving the accuracy and sensitivity of 13C online detection in expiratory air using the TDLAS method in the spectral range of 4860–4880 cm−1. *Laser Phys. Lett.* 15 (10), 105701. doi:10.1088/1612-202x/aad852

Liu, Z., Li, Z., Chen, C., Xu, Z., and He, Y. (2018). A near-infrared carbon dioxide sensor system using a compact folded optical structure for deep-sea natural gas hydrate exploration. *Anal. Methods* 10 (39), 4838–4844. doi:10.1039/C8AY01721F

Ma, W., Yin, W., Huang, T., Zhao, Y., Li, C., and Jia, S. (2004). Theoretical analysis of pressure-dependent peak absorption coefficient for gases. *Spectrosc. Spectr. Analysis* 24 (2), 135–137. doi:10.3321/j.issn:1000-0593.2004.02.003

Ma, Y., Qiao, S., He, Y., and Sun, H. (2024). Ultra-highly sensitive dual gases detection based on photoacoustic spectroscopy by exploiting a long-wave, high-power, wide-tunable, single-longitudinal-mode solid-state laser. *Light Sci. and Appl.* 13, 104. doi:10.1038/s41377-024-01538-7

Ma, Y., Wang, R., He, Y., and Qiao, S. (2025). Highly sensitive laser spectroscopy sensing based on a novel four-prong quartz tuning fork. *Opto-Electronic Adv.* 8 (4), 240187. doi:10.29026/oea.2025.240187

Mandelis, A., and Hess, P. (2017). *Progress in photothermal and photoacoustic science and technology: life and Earth sciences*. Oxford, United Kingdom: Elsevier Science Ltd., 1992.

Meng, Y., Liu, T., Liu, K., Jiang, J., Wang, R., and Wang, T. (2015). Simultaneous detection of mixed gases based on overlapped spectra separation with SLIDT. *IEEE Photonics Technol. Lett.* 27 (7), 794–797. doi:10.1109/LPT.2015.2398875

Rieker, G. B., Jeffries, J. B., and Hanson, R. K. (2009). Calibration-free wavelength-modulation spectroscopy for measurements of gas temperature and concentration in harsh environments. *Appl. Opt.* 48 (29), 5546–5560. doi:10.1364/AO.48.005546

Sigrist, M. W. (2003). Trace gas monitoring by laser-photoacoustic spectroscopy. *Rev. Sci. Instrum.* 74 (1), 486–490. doi:10.1063/1.1512688

Sur, R., Spearrin, R. M., Peng, W. Y., and Hanson, R. K. (2016). Scanned-wavelength-modulation spectroscopy near 2.5 µm for H2O and temperature in a hydrocarbon-fueled scramjet combustor. *J. Quantitative Spectrosc. Radiat. Transf.* 175, 90–104. doi:10.1016/j.jqsrt.2016.02.008

Tian, S. D., Wang, Z., Du, Y. J., Ding, Y. J., and Peng, Z. M. (2023). High-precision measurement of spectral line parameters of CO molecule at 2.3 µm based on wavelength modulation-direct absorption spectroscopy. *Spectrosc. Spectr. Analysis* (7), 2246–2251. doi:10.3964/j.issn.1000-0593(2023)07-2246-06

Wang, H., Zhang, Y., Wang, Z., Li, J., and Liu, Y. (2025). A photoacoustic spectroscopy system for dissolved gases in transformer oil using optimized optical fiber microphone. *Opt. Laser Technol.*, 181. doi:10.1016/j.optlastec.2025.113665

Yang, Y., Li, G., Li, X., and Pan, S. (2017). Partial least squares algorithm application in TDLAS based trace H2S analyses in natural gas. *Acta Photonica Sin.* 46 (2), 0230002. doi:10.3788/gzxb20174602.0230002

Yin, Z. Q., Wu, C., Gong, W. Y., Gong, Z. K., and Wang, Y. J. (2013). Study of the voigt lineshape function and its maximum value. *Acta Phys. Sin.* 62 (12), 123301. doi:10.7498/aps.62.123301

Yu, L., Liu, T., Liu, K., Jiang, J., and Wang, T. (2016). A method for separation of overlapping absorption lines in intracavity gas detection. *Sensors Actuators B Chem.* 228, 10–15. doi:10.1016/j.snb.2015.12.106IEEEPC57.104/D6.2

Zhang, T., Kang, J., Meng, D., Wang, H., Mu, Z., Zhou, M., et al. (2018). Mathematical methods and algorithms for improving near-infrared tunable diode-laser absorption spectroscopy. *Sensors* 18 (12), 4295. doi:10.3390/s18124295